Lifetime Measurements and Triple Coexisting Band Structure in ^{43}S

T. Mijatović,[1,*] N. Kobayashi,[1,†] H. Iwasaki,[1,2] D. Bazin,[1] J. Belarge,[1] P. C. Bender,[1,‡] B. A. Brown,[1,2] A. Dewald,[3] R. Elder,[1,2] B. Elman,[1,2] A. Gade,[1,2] M. Grinder,[1,2] T. Haylett,[4] S. Heil,[5] C. Loelius,[1,2] B. Longfellow,[1,2] E. Lunderberg,[1,2] M. Mathy,[5] K. Whitmore,[1] and D. Weisshaar[1]

[1]*National Superconducting Cyclotron Laboratory, Michigan State University, East Lansing, Michigan 48824, USA*
[2]*Department of Physics and Astronomy, Michigan State University, East Lansing, Michigan 48824, USA*
[3]*Institut für Kernphysik der Universität zu Köln, Köln D-50937, Germany*
[4]*Department of Physics, University of York, Heslington, York YO10 5DD, United Kingdom*
[5]*Institut für Kernphysik, Technische Universität Darmstadt, Darmstadt 64289, Germany*

(Received 23 March 2018; revised manuscript received 7 May 2018; published 5 July 2018)

Lifetime measurements of excited states in the neutron-rich nucleus ^{43}S were performed by applying the recoil-distance method on fast rare-isotope beams in conjunction with the Gamma-Ray Energy Tracking In-beam Nuclear Array. The new data based on $\gamma\gamma$ coincidences and lifetime measurements resolve a doublet of $(3/2^-)$ and $(5/2^-)$ states at low excitation energies. Results were compared to the $\pi(sd) - \nu(pf)$ shell model and antisymmetrized molecular dynamics calculations. The consistency with the theoretical calculations identifies a possible appearance of three coexisting bands near the ground state of ^{43}S: the $K^\pi = 1/2^-$ band built on a prolate-deformed ground state, a band built on an isomer with a $1f_{7/2}^{-1}$ character, and a suggested excited band built on a newly discovered doublet state. The latter further confirms the collapse of the $N = 28$ shell closure in the neutron-rich region.

DOI: 10.1103/PhysRevLett.121.012501

The low-lying structure of atomic nuclei has been characterized by the interplay of the single-particle and collective excitations built on the ground state. The nuclear shape at closed shells tends to be spherical, while collectivity can develop and evolve from vibrational to rotational as moving into the midshell. This picture can be altered in exotic nuclei far from stability where the shell structure drastically changes, and the collective properties can be more diverse even at low excitation energies. Recently, there has been increased interest in the region around the $N = 28$ magic number, where the diminished shell gap is expected to induce strong quadrupole correlations. Excitations across the shell gap can become energetically favored and compete with normal configurations at low excitation energies, exhibiting significantly different collectivity and shape characteristics [1,2]. Thus, the coexistence of various deformed states built on the $1f_{7/2}$ and $2p_{3/2}$ orbits can occur [3]. In fact, experimental data show that stabilizing effects of the $N = 28$ shell gap vanish in neutron-rich isotopes south of the doubly magic ^{48}Ca nucleus; for example, ^{44}S [4] and ^{42}Si [5] display collective behavior and deformation [2,4–6].

Shape and configuration coexistence in the neutron-rich sulfur isotopes has attracted much attention, with results showing a strong competition among different configurations, as well as fairly large collectivity observed in even-even ^{40,42,44}S isotopes [4,7–9]. The collective nature of ^{44}S at $N = 28$ was evidenced from the low-lying 2^+ state and large $B(E2)$ reduced transition probability [4]. Recent studies suggest that the shell erosion in $N = 28$ results in prolate-spherical shape coexistence in the two lowest 0^+ states in ^{44}S [10] and even induces triple configuration coexistence [11] involving an isomeric yrast 4^+ state as a new type of high $K = 4$ isomer with significant triaxiality [12–14]. Therefore, it is important to understand how shape coexistence and collectivity manifest and evolve in neutron-rich odd-mass sulfur isotopes, as coexistence phenomena with important impacts of triaxiality are predicted theoretically [15,16].

The evidence for shape coexistence in ^{43}S with $N = 27$ has been mainly accumulated through the spectroscopy of the isomeric state at 320.5(5) keV [17,18]. A g-factor measurement proved the isomer has the spin and parity $7/2^-$ [18] and suggested it is built on the normal-order $1f_{7/2}$ neutron-hole configuration, while the ground state has a neutron $2p_{3/2}$ intruder nature [17]. The spectroscopic quadrupole moment of the isomeric state was later measured, and found to be larger than expected for a single-particle state [19]. Intruder neutron configurations, driven by the neutron-proton correlations, are suggested to contribute to its wave function [19]. For other excited states, the intermediate-energy Coulomb excitation measurements suggested a level around $E_\gamma \sim 940$ keV [20,21] and knock-out studies extended the level scheme based on energy considerations and observed intensities [22]. Although these studies suggest spherical-prolate shape coexistence [18], it is still essential to experimentally identify the band structure built on top of each coexisting state.

The present Letter attempts to elucidate the band structure of the low-lying states of ^{43}S to get a comprehensive picture of the shape coexistence. Here we present results of $\gamma\gamma$ coincidence data and precise lifetime measurements of excited states in ^{43}S using the recoil-distance method. We determine the electromagnetic transition probabilities, a sensitive probe of collectivity, in a model-independent way. The new results provide the first evidence of a doublet of $(3/2^-)$ and $(5/2^-)$ in ^{43}S. A comparison with the shell model and antisymmetrized molecular dynamics (AMD) calculations is also reported, further confirming experimental findings and indicating the possible appearance of three coexisting bands at the low excitation energies.

The experiment was performed at the Coupled Cyclotron Facility at the National Superconducting Cyclotron Laboratory. The secondary beam of ^{44}Cl was produced from the fragmentation of a 140 MeV/nucleon ^{48}Ca primary beam impinging on a ^{9}Be production target and was separated in the A1900 fragment separator [23]. The secondary beam was used to populate ^{43}S via proton knockout reactions. The projectilelike products were identified in the S800 spectrograph [24] from a correlation of the time of flight with energy losses measured in the S800 focal plane.

Gamma rays emitted at the secondary target location were detected using the Gamma-Ray Energy Tracking In-Beam Nuclear Array (GRETINA) [25,26] in coincidence with the residues. GRETINA consisted of nine detector modules, each detector having four 36-fold segmented high-purity germanium crystals. Four detector modules were positioned at forward angles, covering the laboratory angles of 20°–50° with respect to the beam axis and were used to determine lifetimes.

In this experiment, the excited states of interest were first studied using the 99 MeV/nucleon ^{44}Cl beam on a 2 mm-thick Be target. In a separate run, lifetimes of the excited states were measured with the TRIPLEX device [27] with the 2 mm-thick Be target and 0.58 mm Ta degrader positioned further downstream, using the ^{44}Cl beam at the lower energy of 89 MeV/nucleon. The recoil velocities relative to the speed of light ($\beta = v/c$) were labeled fast ($\beta_{\mathrm{fast}} = 0.377$) and slow ($\beta_{\mathrm{slow}} = 0.297$), denoting the velocity behind the target and degrader, respectively.

The Doppler-shift-corrected γ-ray spectrum of ^{43}S in the target-only setting is shown in Fig. 1. Experimental data are compared to a Monte Carlo simulation (red line) that accurately reproduces all important aspects of the experimental setup [28] and the relative populations were extracted from the comparison. We observe strong transitions at 184(2), 628(5), 977(9), 1159(9), and 1213(10) keV, with the 1159(9) keV transition being the most strongly populated with the inclusive (sum of direct and indirect) population of 37(2)%. Populations to the other four states are around 10%–13%. All of the observed

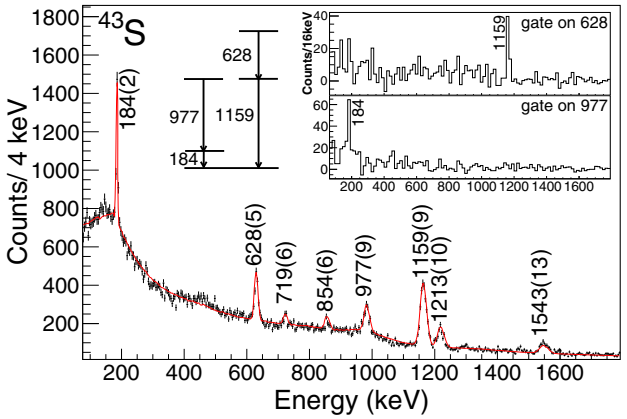

FIG. 1. Doppler-shift-corrected γ-ray spectrum of ^{43}S together with the partial level scheme. Data are compared to the simulated responses for observed transitions (red line). (Insets) Background-subtracted $\gamma\gamma$ spectra in coincidence with the 628 keV (top) and 977 keV (bottom) transitions.

transitions are known from the previous two reaction studies [22], which suggested that an excited state at 1154(7) keV either decays directly to the ground state or undergoes a cascade decay, with the 183(1) keV γ-ray transition followed by the 971(6) keV transition. This conclusion was based solely on the observed intensities and energy considerations [22]. Background-subtracted $\gamma\gamma$ coincidence spectra shown in the insets of Fig. 1 establish several conclusive relationships. The 628 keV transition is observed only in coincidence with the 1159 keV transition. Observed intensities of the 628 and 1159 keV transitions result in the proposed level scheme as shown in Fig. 1. With a gate on the 977 keV line, only the 184 keV transition is clearly visible and vice versa. Coincidence was not observed between the 628 and 977/184 keV transitions, which implies another state should exist at 1161 keV, very close to 1159 keV, and suggests a doublet. Observed intensities of the 184 and 977 keV γ rays are equal to each other within experimental uncertainties in the present and previous measurements [22]. In this work, the order of the 184 and 977 keV transitions can be validated with the lifetime measurements.

The recoil-distance lifetime measurements were performed using three short target-degrader separations: 0, 0.5, and 1 mm. The relative number of reactions occurring on the target and degrader was constrained by moving the foils to 22 mm apart so that there is ample time after each foil for the excited states to decay completely before the next foil is reached. The relative degrader contributions were found to be 12% or smaller. Each lifetime was determined through the χ^2 minimization by comparing data to a set of simulated γ-ray spectra, where only the lifetime of the state was varied. This method was checked by extracting the known lifetime for 2^+ state in ^{42}S. The present result of $21.5^{+1.1}_{-0.9}$ ps is in excellent agreement with the recently published value of 20.6(1.5) ps [12].

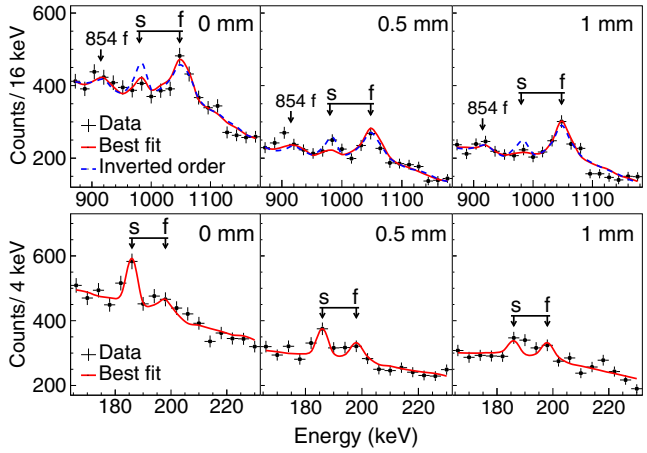

FIG. 2. (Top) Gamma-ray spectrum for the ^{43}S 977 keV transition using 0-, 0.5-, and 1 mm target-to-degrader separations. Identification of the fast (f) and slow (s) components is shown. The data are compared to simulated spectra with the best-fit result of $\tau = 6.2$ ps with the adopted order of the 977 → 184 keV transition. The dashed blue line is given as a reference for the inverted order of the 184 keV ($\tau = 15$ ps) → 977 keV ($\tau = 0.1$ ps) decays. A peak around 920 keV is the fast component of the 854 keV transition. (Bottom) Gamma-ray spectrum for the ^{43}S 184 keV transition. The data are compared to simulated spectra with $\tau = 7.8$ ps for the 184 keV state.

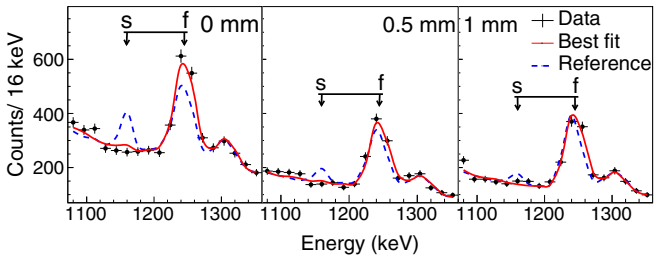

FIG. 3. Gamma-ray spectrum for the ^{43}S 1159 keV transition using 0-, 0.5-, and 1 mm target-to-degrader separations. The data are compared to simulated spectra with the upper limit of 1.5 ps obtained from this experiment and the reference simulated spectra with $\tau = 6.2$ ps that was adapted for the 977 keV transition (dashed curves).

The Doppler-shift-corrected γ-ray spectra obtained with the three separation settings are shown in Fig. 2 for the 977 keV (top) and 184 keV (bottom) transitions. The double peak structure characteristic of decays with lifetimes on the order of 10 ps is noticeable. The 184 keV transition shows more significant slow components, suggesting that the cascade decay precedes with the 977 keV transition, followed by the 184 keV transition, proposing the reversed order from the previous assignment [20,22].

To check the current conclusion on a more quantitative basis, the lifetime for the 1161 keV state is analyzed in more detail based on the cascade decay scenario (977 → 184 keV) proposed in this study. The mean lifetime is determined from the analysis of the 977 keV transition to be $6.2^{+1.4}_{-1.3}(\text{stat})^{+1.3}_{-1.3}(\text{syst})$ ps (Fig. 2, top, red curves). The main systematic errors arise from ambiguities in the target-to-degrader reaction ratio (13%), the population pattern (15%), and the background assumption (10%). If we consider a different cascade scenario in which the 184 keV decay originates from the 1161 keV state, the state lifetime is deduced as 15(2) ps from the 184 keV spectra, and the simulated response (Fig. 2, top, blue curves) cannot reproduce the overall spectra for the 977 keV transition, even when a very short lifetime of 0.1 ps is considered. Note that this scenario (inverted order of Fig. 2) [22] requires the 977 keV transition to proceed via $E2$ transition with the lifetime of 10(4) ps as suggested by the Coulomb excitation measurement [20]. The present conclusion is confirmed by analyzing the overall spectra, where all distance data are summed up to reduce statistical uncertainties, which resulted in the minimum χ^2 of 19.5 ($N_{df} = 20$) for the currently adopted scenario (977 → 184 keV) compared to χ^2 of 31 for the inverted order [20,22]. In Fig. 2, individual spectra agree very well with the current scenario except for the 0.5 mm data, which is likely due to the statistical uncertainty.

The lifetime of the 184 keV state was determined after taking into account the feeding contributions from the 977 keV decay. The result is found to be $7.8^{+1.4}_{-1.3}(\text{syst})^{+1.3}_{-1.6}(\text{syst})$ ps as shown in Fig. 2 (bottom, in red). The main systematic errors in this case were from ambiguities in the target-to-degrader reaction ratio (12%) and the uncertainty of the lifetime of the 1161 keV state (17%).

Finally, the lifetime of the 1159 keV state was studied as shown in Fig. 3. If the 977 keV transition depopulates the 1159 keV state, the lifetime should be equal to 6.2 ps, which is shown by the blue curves. Obviously, the present data disagree with the lifetime of 6.2 ps for the 1159 keV state and indicate a much shorter lifetime with the upper limit of 1.5 ps with one sigma upper bound of the statistical error. This result confirms a doublet, with independent states occurring at 1159 and 1161 keV.

Based on the measured lifetimes and $\gamma\gamma$ coincidence information, we propose the level scheme in Fig. 4. Data are compared to the shell model calculations, which were carried out in the $\pi(sd) - \nu(pf)$ basis with the SDPF-U [29] and SDPF-MU [30] Hamiltonian using the code NUSHELLX [31]. The $M1$ effective operator for protons in the sd shell [32] and neutrons in the pf shell [33] is included using $g_s^p = 5.0$, $g_s^n = -3.443$, $g_l^p = 1.174$, $g_l^n = -0.1$, and $g_t^p = 0.24$, $g_t^n = 0.0$. The $E2$ effective charges are $e_p = 1.5e$ and $e_n = 0.5e$. Spectroscopic factors C^2S for one-proton removal from the assumed 2^- ground state of ^{44}Cl [34] were also calculated. Both shell model calculations predict very similar structure for ^{43}S, as shown in Table I, and the results from the SDPF-U calculations are illustrated in Fig. 4. The present results conclude that the 1161 keV state

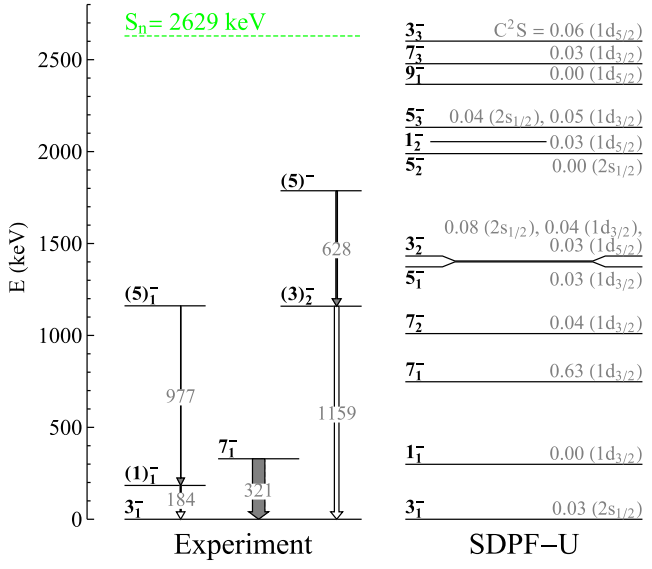

FIG. 4. Comparison of the experimental level scheme with results of the SDPF-U shell model calculations. The states are labeled by twice their spin value ($2J$). The 1787 keV level is considered as the theoretical $5/2_3^-$ state. Spectroscopic factors C^2S for dominant ($C^2S_{\max}$) or strong ($C^2S > 0.03$) knockout channels are shown on the far right together with the single-particle orbitals for proton removal. The $M1$ transitions are denoted by empty arrows. The $E2$ transitions are denoted by gray arrows.

TABLE I. Comparison between the experimental data and the shell-model calculations for energies, reduced transition probabilities and branching ratios. All energies are given in keV, $B(M1)$ in μ_N^2 and $B(E2)$ in $e^2\mathrm{fm}^4$. For the reduced transition probability results, statistical and systematic errors are added in quadrature. The shell-model predictions of the spectroscopic quadrupole moments are given in units of $e\mathrm{fm}^2$.

Observable	Experiment	SDPF-U	SDPF-MU
$E(1/2_1^-)$	184(2)	299	135
$E(7/2_1^-)$	320.5(5)	748	601
$E(5/2_1^-)$	1161(11)	1400	1035
$E(3/2_2^-)$	1159(9)	1405	875
$E(5/2_3^-)$	1787(14)	2132	2198
$B(E2, 7/2_1^- \to 3/2_1^-)$	0.403(8) [18]	2.25	2.93
$B(M1, 1/2_1^- \to 3/2_1^-)$	$1.2^{+0.3}_{-0.3}$	0.65	0.38
$B(E2, 1/2_1^- \to 3/2_1^-)$		219	204
$B(E2, 5/2_1^- \to 1/2_1^-)$	146^{+45}_{-42}	113	107
$B(M1, 3/2_2^- \to 3/2_1^-)$	> 0.02[a]	0.03	0.04
$B(E2, 3/2_2^- \to 3/2_1^-)$		6.28	24.4
$Q(3/2_1^-)$		−15.4	−14.0
$Q(7/2_1^-)$		29.6	30.7
$Q(5/2_1^-)$		−18.9	−18.3
$Q(3/2_2^-)$		13.1	11.5
$Q(5/2_3^-)$		2.2	23.0
$\mathrm{BR}(5/2_3^- \to 7/2_1^-)$	< 20	7	24
$\mathrm{BR}(5/2_3^- \to 5/2_1^-)$	< 3	10	2

[a]Assuming pure $M1$ transition.

deexcites via 977 keV γ rays populating the 184 keV state. This observation is consistent with the cascade transition from the $5/2_1^-$ state, $5/2_1^- \to 1/2_1^- \to 3/2_{gs}^-$, suggested by the shell model, since other neighboring states such as $7/2_2^-$ and $3/2_2^-$ strongly favor the direct decays to the ground state. The state observed at 184 keV is therefore suggested to be $1/2_1^-$ as the bandhead of the $K^\pi = 1/2^-$ band, which was missing in the previous assignment [22]. The calculated spectroscopic factor for the $1/2_1^-$ is close to zero, which is in agreement with the negligible direct population observed in this work. The calculations also predict that the $5/2_1^-$ and $7/2_2^-$ states are members of the ground-state band, although the population to the previously proposed $7/2_2^-$ state at 920–940 keV [20,21] was not observed in this work. Besides, the shell model predicts the $7/2_1^-$ isomer at a somewhat higher energy than experimentally observed [18,19]. This state is calculated to have the largest spectroscopic factor because of its strong single neutron-hole component. Finally, the SDPF-U shell model calculations predict a $(5/2_1^-, 3/2_2^-)$ doublet around 1400 keV with a different sign of quadrupole moments (Table I), suggesting different intrinsic shapes for these states. The larger spectroscopic factor predicted for the $3/2_2^-$ state is consistent with the observed population that favors the 1159 keV state.

Experimental transition probabilities are extracted from the measured lifetimes and the proposed level scheme. The consistency between the measured and calculated transition probabilities further confirms the present level scheme assignment. The cascade decay of the 1161 keV state starts with the $E2$ decay to the proposed $1/2_1^-$ state at 184 keV, which decays further to the $3/2_{gs}^-$ with a dominant $M1$ transition. The 6.2 ps lifetime of the 1161 keV state corresponds to the reduced transition probability of $B(E2, 5/2^- \to 1/2^-) = 146^{+32}_{-31}(\mathrm{stat})^{+31}_{-31}(\mathrm{syst})\ e^2\mathrm{fm}^4$, assuming the branching ratio of 100% for the $5/2_1^-$ decay to the $1/2_1^-$ state. As for the 184 keV transition, the decay should predominantly occur via the $M1$ transition based on the small level spacings and the spin-parity combination suggested from the level scheme (Fig. 4), leading to $B(M1, 1/2^- \to 3/2^-) = 1.2^{+0.2}_{-0.2}(\mathrm{stat})^{+0.2}_{-0.3}(\mathrm{syst})\ \mu_N^2$. The 1159 keV state decays directly to the ground state, with the strong 628 keV transition observed on top of it, as suggested from the coincidence considerations. The 1159 keV state is observed to have a short lifetime (< 1.5 ps) and is most likely the $3/2_2^-$ state with the predicted lifetime of 1.2 ps. The shell model suggests this state as a candidate for the other bandhead with the positive spectroscopic quadrupole moment (Table I). The 628 keV transition is proposed as the fast $5/2_3^- \to 3/2_2^-$ transition, since the observed population to the 1787 keV state is consistent with the large spectroscopic factor for the $5/2_3^-$ state.

Possible interband transitions were studied for the 1787 keV state to examine the band structure and results are shown in Table I. The spectrum (Fig. 1) shows a hint of the 1467 keV transition, which is consistent with the decay of the 1787 keV state to the isomeric $7/2_1^-$ state. If this is the case, the estimated branching ratio is about 20%, although the decay to the $3/2_2^-$ state is still dominant. In addition, the upper limit of 3% is obtained for the decay from the 1787 keV state to the 1161 keV state based on the coincidence data (Fig. 1). Each excited state decays preferentially through the band, even though calculations suggest several intraband transitions.

The triple band structure in ^{43}S has been consistently predicted by both shell model and antisymmetrized molecular dynamics calculations, with a different interpretation of the nature of the third excited band built on the $3/2_2^-$ state [15,16]. The recent shell model calculations by Chevrier and Gaudefroy [15] suggest that the axially prolate-deformed ground-state band coexists with a triaxial band built on the $7/2_1^-$ isomer and an excited prolate structure built on the $K^\pi = 5/2^-$ deformed orbit. The $3/2_2^-$ state, predicted to have a large asymmetry parameter $\gamma = 28°$, is considered as the decay path of the prolate $K^\pi = 5/2^-$ band built on the $5/2_2^-$ state.

An alternative interpretation of the third excited band with the significantly different $K^\pi = 3/2^-$ oblate configuration is given by the AMD calculations by Kimura *et al.* [16]. This third oblate-deformed band is predicted to start with the $3/2_2^-$ at 1800 keV, leading to a triple shape coexistence with the prolate-deformed ground-state band and a triaxially deformed isomeric state. At the large prolate deformation, the intruder $(\nu 2p_{3/2})^1$ configuration dominates, whereas on the oblate side, the normal $(\nu 1f_{7/2})^{-1}$ configuration dominates with the pronounced magicity. Both normal and intruder configurations coexist in the triaxial region because of the enhanced quadrupole correlation triggered by the quenching of the $N = 28$ shell gap.

In summary, the model-independent lifetime measurements were performed for the excited states of ^{43}S by applying the recoil-distance method with GRETINA. Our results confirm a doublet at around 1.2 MeV and agree well with theoretical predictions for triple band coexistence, presenting the complexity of nuclear many-body systems. Results further confirm a collapse of the $N = 28$ shell closure highlighting the importance of nuclear structure studies in this neutron-rich region.

The authors thank the beam physicists at the Coupled Cyclotron Facility for the delivery of the radioactive beam. This work is supported by the National Science Foundation (NSF) under PHY-1102511 and PHY-1565546, by the Department of Energy (DOE) National Nuclear Security Administration under Awards No. DE-NA0003180 and No. DE-NA0000979, and also partly by the DFG under Contract No. DE 1516/3-1. GRETINA was funded by the DOE, Office of Science. Operation of the array at NSCL was supported by DOE under Grants No. DE-SC0014537 (NSCL) and No. DE-AC02-05CH11231 (LBNL).

*mijatovi@nscl.msu.edu
†Present address: Research Center for Nuclear Physics (RCNP), Osaka University, Ibaraki, Osaka 567-0047, Japan.
‡Present address: Department of Physics, University of Massachusetts Lowell, Lowell, Massachusetts 01854, USA.

[1] K. Heyde and J. L. Wood, Rev. Mod. Phys. **83**, 1467 (2011).
[2] A. Gade and S. N. Liddick, J. Phys. G **43**, 024001 (2016).
[3] O. Sorlin and M.-G. Porquet, Prog. Part. Nucl. Phys. **61**, 602 (2008).
[4] T. Glasmacher, B. A. Brown, M. J. Chromik, P. D. Cottle, M. Fauerbach, R. W. Ibbotson, K. W. Kemper, D. J. Morrissey, H. Scheit, D. W. Sklenicka, and M. Steiner, Phys. Lett. B **395**, 163 (1997).
[5] B. Bastin *et al.*, Phys. Rev. Lett. **99**, 022503 (2007).
[6] S. Takeuchi *et al.*, Phys. Rev. Lett. **109**, 182501 (2012).
[7] H. Scheit, T. Glasmacher, B. A. Brown, J. A. Brown, P. D. Cottle, P. G. Hansen, R. Harkewicz, M. Hellström, R. W. Ibbotson, J. K. Jewell, K. W. Kemper, D. J. Morrissey, M. Steiner, P. Thirolf, and M. Thoennessen, Phys. Rev. Lett. **77**, 3967 (1996).
[8] L. Gaudefroy, Phys. Rev. C **81**, 064329 (2010).
[9] E. Lunderberg, A. Gade, V. Bader, T. Baugher, D. Bazin, J. S. Berryman, B. A. Brown, D. J. Hartley, F. Recchia, S. R. Stroberg, D. Weisshaar, and K. Wimmer, Phys. Rev. C **94**, 064327 (2016).
[10] C. Force *et al.*, Phys. Rev. Lett. **105**, 102501 (2010).
[11] D. Santiago-Gonzalez, I. Wiedenhöver, V. Abramkina, M. L. Avila, T. Baugher, D. Bazin, B. A. Brown, P. D. Cottle, A. Gade, T. Glasmacher, K. W. Kemper, S. McDaniel, A. Rojas, A. Ratkiewicz, R. Meharchand, E. C. Simpson, J. A. Tostevin, A. Volya, and D. Weisshaar, Phys. Rev. C **83**, 061305(R) (2011).
[12] J. J. Parker IV *et al.*, Phys. Rev. Lett. **118**, 052501 (2017).
[13] Y. Utsuno, N. Shimizu, T. Otsuka, T. Yoshida, and Y. Tsunoda, Phys. Rev. Lett. **114**, 032501 (2015).
[14] J. L. Egido, M. Borrajo, and T. R. Rodríguez, Phys. Rev. Lett. **116**, 052502 (2016).
[15] R. Chevrier and L. Gaudefroy, Phys. Rev. C **89**, 051301(R) (2014).
[16] M. Kimura, Y. Taniguchi, Y. Kanada-En'yo, H. Horiuchi, and K. Ikeda, Phys. Rev. C **87**, 011301(R) (2013).
[17] F. Sarazin *et al.*, Phys. Rev. Lett. **84**, 5062 (2000).
[18] L. Gaudefroy *et al.*, Phys. Rev. Lett. **102**, 092501 (2009).
[19] R. Chevrier *et al.*, Phys. Rev. Lett. **108**, 162501 (2012).
[20] R. W. Ibbotson, T. Glasmacher, P. F. Mantica, and H. Scheit, Phys. Rev. C **59**, 642 (1999).
[21] S. Calinescu *et al.*, J. Phys. Conf. Ser. **413** (2013) 012030.
[22] L. A. Riley, P. Adrich, T. R. Baugher, D. Bazin, B. A. Brown, J. M. Cook, P. D. Cottle, C. Aa. Diget, A. Gade, D. A. Garland, T. Glasmacher, K. E. Hosier, K. W. Kemper,

A. Ratkiewicz, K. P. Siwek, J. A. Tostevin, and D. Weisshaar, Phys. Rev. C **80**, 037305 (2009).
[23] D. J. Morrissey, B. M. Sherrill, M. Steiner, A. Stolz, and I. Wiedenhoever, Nucl. Instrum. Methods Phys. Res., Sect. B **204**, 90 (2003).
[24] D. Bazin, J. A. Caggiano, B. M. Sherrill, J. Yurkon, and A. Zeller, Nucl. Instrum. Methods Phys. Res., Sect. B **204**, 629 (2003).
[25] S. Paschalis *et al.*, Nucl. Instrum. Methods Phys. Res., Sect. A **709**, 44 (2013).
[26] D. Weisshaar *et al.*, Nucl. Instrum. Methods Phys. Res., Sect. A **847**, 187 (2017).
[27] H. Iwasaki, A. Dewald, T. Braunroth, C. Fransen, D. Smalley, A. Lemasson, C. Morse, K. Whitmore, and C. Loelius, Nucl. Instrum. Methods Phys. Res., Sect. A **806**, 123 (2016).
[28] P. Adrich, D. Enderich, D. Miller, V. Moeller, R. Norris, K. Starosta, C. Vaman, P. Voss, and A. Dewald, Nucl. Instrum. Methods Phys. Res., Sect. A **598**, 454 (2009).
[29] F. Nowacki and A. Poves, Phys. Rev. C **79**, 014310 (2009).
[30] Y. Utsuno, T. Otsuka, B. A. Brown, M. Honma, T. Mizusaki, and N. Shimizu, Phys. Rev. C **86**, 051301 (2012).
[31] NUSHELLX, http://www.garsington.eclipse.co.uk/.
[32] W. A. Richter, S. Mkhize, and B. A. Brown, Phys. Rev. C **78**, 064302 (2008).
[33] M. Honma, T. Otsuka, B. A. Brown, and T. Mizusaki, Phys. Rev. C **69**, 034335 (2004).
[34] M. De Rydt, J. M. Daugas, F. de Oliveira Santos, L. Gaudefroy, S. Grévy, D. Kameda, V. Kumar, R. Lozeva, T. J. Mertzimekis, P. Morel, T. Nagatomo, G. Neyens, L. Perrot, O. Sorlin, C. Stödel, J. C. Thomas, N. Vermeulen, and P. Vingerhoets, Phys. Rev. C **81**, 034308 (2010).